

Measurement of $d\sigma/dM$ and Forward-Backward Charge Asymmetry for High Mass Drell-Yan e^+e^- Pairs from $p\bar{p}$ Collisions at $\sqrt{s} = 1.8$ TeV

T. Affolder,²³ H. Akimoto,⁴⁵ A. Akopian,³⁷ M. G. Albrow,¹¹ P. Amaral,⁸ D. Amidei,²⁵ K. Anikeev,²⁴ J. Antos,¹ G. Apollinari,¹¹ T. Arisawa,⁴⁵ A. Artikov,⁹ T. Asakawa,⁴³ W. Ashmanskas,⁸ F. Azfar,³⁰ P. Azzi-Bacchetta,³¹ N. Bacchetta,³¹ H. Bachacou,²³ S. Bailey,¹⁶ P. de Barbaro,³⁶ A. Barbaro-Galtieri,²³ V. E. Barnes,³⁵ B. A. Barnett,¹⁹ S. Baroiant,⁵ M. Barone,¹³ G. Bauer,²⁴ F. Bedeschi,³³ S. Belforte,⁴² W. H. Bell,¹⁵ G. Bellettini,³³ J. Bellinger,⁴⁶ D. Benjamin,¹⁰ J. Bensinger,⁴ A. Beretvas,¹¹ J. P. Berge,¹¹ J. Berryhill,⁸ A. Bhatti,³⁷ M. Binkley,¹¹ D. Bisello,³¹ M. Bishai,¹¹ R. E. Blair,² C. Blocker,⁴ K. Bloom,²⁵ B. Blumenfeld,¹⁹ S. R. Blusk,³⁶ A. Bocci,³⁷ A. Bodek,³⁶ W. Bokhari,³² G. Bolla,³⁵ Y. Bonushkin,⁶ D. Bortoletto,³⁵ J. Boudreau,³⁴ A. Brandl,²⁷ S. van den Brink,¹⁹ C. Bromberg,²⁶ M. Brozovic,¹⁰ E. Brubaker,²³ N. Bruner,²⁷ E. Buckley-Geer,¹¹ J. Budagov,⁹ H. S. Budd,³⁶ K. Burkett,¹⁶ G. Busetto,³¹ A. Byon-Wagner,¹¹ K. L. Byrum,² S. Cabrera,¹⁰ P. Calafiura,²³ M. Campbell,²⁵ W. Carithers,²³ J. Carlson,²⁵ D. Carlsmith,⁴⁶ W. Caskey,⁵ A. Castro,³ D. Cauz,⁴² A. Cerri,³³ A. W. Chan,¹ P. S. Chang,¹ P. T. Chang,¹ J. Chapman,²⁵ C. Chen,³² Y. C. Chen,¹ M. -T. Cheng,¹ M. Chertok,⁵ G. Chiarelli,³³ I. Chirikov-Zorin,⁹ G. Chlachidze,⁹ F. Chlebana,¹¹ L. Christofek,¹⁸ M. L. Chu,¹ Y. S. Chung,³⁶ C. I. Ciobanu,²⁸ A. G. Clark,¹⁴ A. Connolly,²³ J. Conway,³⁸ M. Cordelli,¹³ J. Cranshaw,⁴⁰ R. Cropp,⁴¹ R. Culbertson,¹¹ D. Dagenhart,⁴⁴ S. D'Auria,¹⁵ F. DeJongh,¹¹ S. Dell'Agnello,¹³ M. Dell'Orso,³³ L. Demortier,³⁷ M. Deninno,³ P. F. Derwent,¹¹ T. Devlin,³⁸ J. R. Dittmann,¹¹ A. Dominguez,²³ S. Donati,³³ J. Done,³⁹ M. D'Onofrio,³³ T. Dorigo,¹⁶ N. Eddy,¹⁸ K. Einsweiler,²³ J. E. Elias,¹¹ E. Engels, Jr.,³⁴ R. Erbacher,¹¹ D. Errede,¹⁸ S. Errede,¹⁸ Q. Fan,³⁶ R. G. Feild,⁴⁷ J. P. Fernandez,¹¹ C. Ferretti,³³ R. D. Field,¹² I. Fiori,³ B. Flaughner,¹¹ G. W. Foster,¹¹ M. Franklin,¹⁶ J. Freeman,¹¹ J. Friedman,²⁴ Y. Fukui,²² I. Furic,²⁴ S. Galeotti,³³ A. Gallas,^(**) 16 M. Gallinaro,³⁷ T. Gao,³² M. Garcia-Sciveres,²³ A. F. Garfinkel,³⁵ P. Gatti,³¹ C. Gay,⁴⁷ D. W. Gerdes,²⁵ P. Giannetti,³³ P. Giromini,¹³ V. Glagolev,⁹ D. Glenzinski,¹¹ M. Gold,²⁷ J. Goldstein,¹¹ I. Gorelov,²⁷ A. T. Goshaw,¹⁰ Y. Gotra,³⁴ K. Goulianos,³⁷ C. Green,³⁵ G. Grim,⁵ P. Gris,¹¹ L. Groer,³⁸ C. Grosso-Pilcher,⁸ M. Guenther,³⁵ G. Guillian,²⁵ J. Guimaraes da Costa,¹⁶ R. M. Haas,¹² C. Haber,²³ S. R. Hahn,¹¹ C. Hall,¹⁶ T. Handa,¹⁷ R. Handler,⁴⁶ W. Hao,⁴⁰ F. Happacher,¹³ K. Hara,⁴³ A. D. Hardman,³⁵ R. M. Harris,¹¹ F. Hartmann,²⁰ K. Hatakeyama,³⁷ J. Hauser,⁶ J. Heinrich,³² A. Heiss,²⁰ M. Herndon,¹⁹ C. Hill,⁵ K. D. Hoffman,³⁵ C. Holck,³² R. Hollebeek,³² L. Holloway,¹⁸ R. Hughes,²⁸ J. Huston,²⁶ J. Huth,¹⁶ H. Ikeda,⁴³ J. Incandela,¹¹ G. Introzzi,³³ J. Iwai,⁴⁵ Y. Iwata,¹⁷ E. James,²⁵ M. Jones,³² U. Joshi,¹¹ H. Kambara,¹⁴ T. Kamon,³⁹ T. Kaneko,⁴³ K. Karr,⁴⁴ H. Kasha,⁴⁷ Y. Kato,²⁹ T. A. Keaffaber,³⁵ K. Kelley,²⁴ M. Kelly,²⁵ R. D. Kennedy,¹¹ R. Kephart,¹¹ D. Khazins,¹⁰ T. Kikuchi,⁴³ B. Kilminster,³⁶ B. J. Kim,²¹ D. H. Kim,²¹ H. S. Kim,¹⁸ M. J. Kim,²¹ S. B. Kim,²¹ S. H. Kim,⁴³ Y. K. Kim,²³ M. Kirby,¹⁰ M. Kirk,⁴ L. Kirsch,⁴ S. Klimenko,¹² P. Koehn,²⁸ K. Kondo,⁴⁵ J. Konigsberg,¹² A. Korn,²⁴ A. Korytov,¹² E. Kovacs,² J. Kroll,³² M. Kruse,¹⁰ S. E. Kuhlmann,² K. Kurino,¹⁷ T. Kuwabara,⁴³ A. T. Laasanen,³⁵ N. Lai,⁸ S. Lami,³⁷ S. Lammel,¹¹ J. Lancaster,¹⁰ M. Lancaster,²³ R. Lander,⁵ A. Lath,³⁸ G. Latino,³³ T. LeCompte,² A. M. Lee IV,¹⁰ K. Lee,⁴⁰ S. Leone,³³ J. D. Lewis,¹¹ M. Lindgren,⁶ T. M. Liss,¹⁸ J. B. Liu,³⁶ Y. C. Liu,¹ D. O. Litvintsev,¹¹ O. Lobban,⁴⁰ N. Lockyer,³² J. Loken,³⁰ M. Loreti,³¹ D. Lucchesi,³¹ P. Lukens,¹¹ S. Lusin,⁴⁶ L. Lyons,³⁰ J. Lys,²³ R. Madrak,¹⁶ K. Maeshima,¹¹ P. Maksimovic,¹⁶ L. Malferrari,³ M. Mangano,³³ M. Mariotti,³¹ G. Martignon,³¹ A. Martin,⁴⁷ J. A. J. Matthews,²⁷ J. Mayer,⁴¹ P. Mazzanti,³ K. S. McFarland,³⁶ P. McIntyre,³⁹ E. McKigney,³² M. Menguzzato,³¹ A. Menzione,³³ C. Mesropian,³⁷ A. Meyer,¹¹ T. Miao,¹¹ R. Miller,²⁶ J. S. Miller,²⁵ H. Minato,⁴³ S. Miscetti,¹³ M. Mishina,²² G. Mitselmakher,¹² N. Moggi,³ E. Moore,²⁷ R. Moore,²⁵ Y. Morita,²² T. Moulík,³⁵ M. Mulhearn,²⁴ A. Mukherjee,¹¹ T. Muller,²⁰ A. Munar,³³ P. Murat,¹¹ S. Murgia,²⁶ J. Nachtman,⁶ V. Nagaslaev,⁴⁰ S. Nahn,⁴⁷ H. Nakada,⁴³ I. Nakano,¹⁷ C. Nelson,¹¹ T. Nelson,¹¹ C. Neu,²⁸ D. Neuberger,²⁰ C. Newman-Holmes,¹¹ C.-Y. P. Ngan,²⁴ H. Niu,⁴ L. Nodulman,² A. Nomerotski,¹² S. H. Oh,¹⁰ Y. D. Oh,²¹ T. Ohmoto,¹⁷ T. Ohsugi,¹⁷ R. Oishi,⁴³ T. Okusawa,²⁹ J. Olsen,⁴⁶ W. Orejudos,²³ C. Pagliarone,³³ F. Palmonari,³³ R. Paoletti,³³ V. Papadimitriou,⁴⁰ D. Partos,⁴ J. Patrick,¹¹ G. Pauletta,⁴² M. Paulini,^(*) 23 C. Paus,²⁴ D. Pellett,⁵ L. Pescara,³¹ T. J. Phillips,¹⁰ G. Piacentino,³³ K. T. Pitts,¹⁸ A. Pompos,³⁵ L. Pondrom,⁴⁶ G. Pope,³⁴ M. Popovic,⁴¹ F. Prokoshin,⁹ J. Proudfoot,² F. Ptohos,¹³ O. Pukhov,⁹ G. Punzi,³³ A. Rakitine,²⁴ F. Ratnikov,³⁸ D. Reher,²³ A. Reichold,³⁰ A. Ribon,³¹ W. Riegler,¹⁶ F. Rimondi,³ L. Ristori,³³ M. Riveline,⁴¹ W. J. Robertson,¹⁰ A. Robinson,⁴¹ T. Rodrigo,⁷ S. Rolli,⁴⁴ L. Rosenson,²⁴ R. Roser,¹¹ R. Rossin,³¹ A. Roy,³⁵ A. Ruiz,⁷ A. Safonov,⁵ R. St. Denis,¹⁵ W. K. Sakumoto,³⁶ D. Saltzberg,⁶ C. Sanchez,²⁸ A. Sansoni,¹³ L. Santi,⁴² H. Sato,⁴³ P. Savard,⁴¹ P. Schlabach,¹¹ E. E. Schmidt,¹¹ M. P. Schmidt,⁴⁷ M. Schmitt,^(**) 16 L. Scodellaro,³¹ A. Scott,⁶ A. Scribano,³³ S. Segler,¹¹ S. Seidel,²⁷ Y. Seiya,⁴³ A. Semenov,⁹ F. Semeria,³ T. Shah,²⁴ M. D. Shapiro,²³ P. F. Shepard,³⁴ T. Shibayama,⁴³ M. Shimojima,⁴³ M. Shochet,⁸ A. Sidoti,³¹ J. Siegrist,²³ A. Sill,⁴⁰ P. Sinervo,⁴¹ P. Singh,¹⁸ A. J. Slaughter,⁴⁷ K. Sliwa,⁴⁴ C. Smith,¹⁹ F. D. Snider,¹¹ A. Solodsky,³⁷ J. Spalding,¹¹ T. Speer,¹⁴ P. Sphicas,²⁴ F. Spinella,³³ M. Spiropulu,¹⁶ L. Spiegel,¹¹ J. Steele,⁴⁶ A. Stefanini,³³ J. Strologas,¹⁸ F. Strumia,¹⁴ D. Stuart,¹¹ K. Sumorok,²⁴ T. Suzuki,⁴³ T. Takano,²⁹ R. Takashima,¹⁷ K. Takikawa,⁴³ P. Tamburello,¹⁰ M. Tanaka,⁴³

B. Tannenbaum,⁶ M. Tecchio,²⁵ R. Tesarek,¹¹ P. K. Teng,¹ K. Terashi,³⁷ S. Tether,²⁴ A. S. Thompson,¹⁵ R. Thurman-Keup,² P. Tipton,³⁶ S. Tkaczyk,¹¹ D. Toback,³⁹ K. Tollefson,³⁶ A. Tollestrup,¹¹ D. Tonelli,³³ H. Toyoda,²⁹ W. Trischuk,⁴¹ J. F. de Troconiz,¹⁶ J. Tseng,²⁴ N. Turini,³³ F. Ukegawa,⁴³ T. Vaiciulis,³⁶ J. Valls,³⁸ S. Vejcik III,¹¹ G. Velev,¹¹ G. Veramendi,²³ R. Vidal,¹¹ I. Vila,⁷ R. Vilar,⁷ I. Volobouev,²³ M. von der Mey,⁶ D. Vucinic,²⁴ R. G. Wagner,² R. L. Wagner,¹¹ N. B. Wallace,³⁸ Z. Wan,³⁸ C. Wang,¹⁰ M. J. Wang,¹ B. Ward,¹⁵ S. Waschke,¹⁵ T. Watanabe,⁴³ D. Waters,³⁰ T. Watts,³⁸ R. Webb,³⁹ H. Wenzel,²⁰ W. C. Wester III,¹¹ A. B. Wicklund,² E. Wicklund,¹¹ T. Wilkes,⁵ H. H. Williams,³² P. Wilson,¹¹ B. L. Winer,²⁸ D. Winn,²⁵ S. Wolbers,¹¹ D. Wolinski,²⁵ J. Wolinski,²⁶ S. Wolinski,²⁵ S. Worm,²⁷ X. Wu,¹⁴ J. Wyss,³³ W. Yao,²³ G. P. Yeh,¹¹ P. Yeh,¹ J. Yoh,¹¹ C. Yosef,²⁶ T. Yoshida,²⁹ I. Yu,²¹ S. Yu,³² Z. Yu,⁴⁷ A. Zanetti,⁴² F. Zetti,²³ and S. Zucchelli³

(CDF Collaboration)

¹ *Institute of Physics, Academia Sinica, Taipei, Taiwan 11529, Republic of China*

² *Argonne National Laboratory, Argonne, Illinois 60439*

³ *Istituto Nazionale di Fisica Nucleare, University of Bologna, I-40127 Bologna, Italy*

⁴ *Brandeis University, Waltham, Massachusetts 02254*

⁵ *University of California at Davis, Davis, California 95616*

⁶ *University of California at Los Angeles, Los Angeles, California 90024*

⁷ *Instituto de Fisica de Cantabria, CSIC-University of Cantabria, 39005 Santander, Spain*

⁸ *Enrico Fermi Institute, University of Chicago, Chicago, Illinois 60637*

⁹ *Joint Institute for Nuclear Research, RU-141980 Dubna, Russia*

¹⁰ *Duke University, Durham, North Carolina 27708*

¹¹ *Fermi National Accelerator Laboratory, Batavia, Illinois 60510*

¹² *University of Florida, Gainesville, Florida 32611*

¹³ *Laboratori Nazionali di Frascati, Istituto Nazionale di Fisica Nucleare, I-00044 Frascati, Italy*

¹⁴ *University of Geneva, CH-1211 Geneva 4, Switzerland*

¹⁵ *Glasgow University, Glasgow G12 8QQ, United Kingdom*

¹⁶ *Harvard University, Cambridge, Massachusetts 02138*

¹⁷ *Hiroshima University, Higashi-Hiroshima 724, Japan*

¹⁸ *University of Illinois, Urbana, Illinois 61801*

¹⁹ *The Johns Hopkins University, Baltimore, Maryland 21218*

²⁰ *Institut für Experimentelle Kernphysik, Universität Karlsruhe, 76128 Karlsruhe, Germany*

²¹ *Center for High Energy Physics: Kyungpook National University, Taegu 702-701; Seoul National University, Seoul 151-742; and SungKyunKwan University, Suwon 440-746; Korea*

²² *High Energy Accelerator Research Organization (KEK), Tsukuba, Ibaraki 305, Japan*

²³ *Ernest Orlando Lawrence Berkeley National Laboratory, Berkeley, California 94720*

²⁴ *Massachusetts Institute of Technology, Cambridge, Massachusetts 02139*

²⁵ *University of Michigan, Ann Arbor, Michigan 48109*

²⁶ *Michigan State University, East Lansing, Michigan 48824*

²⁷ *University of New Mexico, Albuquerque, New Mexico 87131*

²⁸ *The Ohio State University, Columbus, Ohio 43210*

²⁹ *Osaka City University, Osaka 588, Japan*

³⁰ *University of Oxford, Oxford OX1 3RH, United Kingdom*

³¹ *Universita di Padova, Istituto Nazionale di Fisica Nucleare, Sezione di Padova, I-35131 Padova, Italy*

³² *University of Pennsylvania, Philadelphia, Pennsylvania 19104*

³³ *Istituto Nazionale di Fisica Nucleare, University and Scuola Normale Superiore of Pisa, I-56100 Pisa, Italy*

³⁴ *University of Pittsburgh, Pittsburgh, Pennsylvania 15260*

³⁵ *Purdue University, West Lafayette, Indiana 47907*

³⁶ *University of Rochester, Rochester, New York 14627*

³⁷ *Rockefeller University, New York, New York 10021*

³⁸ *Rutgers University, Piscataway, New Jersey 08855*

³⁹ *Texas A&M University, College Station, Texas 77843*

⁴⁰ *Texas Tech University, Lubbock, Texas 79409*

⁴¹ *Institute of Particle Physics, University of Toronto, Toronto M5S 1A7, Canada*

⁴² *Istituto Nazionale di Fisica Nucleare, University of Trieste/ Udine, Italy*

⁴³ *University of Tsukuba, Tsukuba, Ibaraki 305, Japan*

⁴⁴ *Tufts University, Medford, Massachusetts 02155*

⁴⁵ *Waseda University, Tokyo 169, Japan*

⁴⁶ *University of Wisconsin, Madison, Wisconsin 53706*

⁴⁷ *Yale University, New Haven, Connecticut 06520*

(*) *Now at Carnegie Mellon University, Pittsburgh, Pennsylvania 15213*
(**) *Now at Northwestern University, Evanston, Illinois 60208*

We report on a measurement of the mass dependence of the forward-backward charge asymmetry, A_{FB} , and production cross section $d\sigma/dM$ for e^+e^- pairs with mass $M_{ee} > 40 \text{ GeV}/c^2$. The data sample consists of 108 pb^{-1} of $p\bar{p}$ collisions at $\sqrt{s} = 1.8 \text{ TeV}$ taken by the Collider Detector at Fermilab during 1992–1995. The measured asymmetry and $d\sigma/dM$ are compared with the predictions of the Standard Model and a model with an extra Z' gauge boson.

PACS numbers: 13.85.Qk, 12.38.Qk, 12.15.Ji, 12.15.Mm, 12.60.-i, 12.60.Cn

In hadron-hadron collisions at high energies, massive e^+e^- pairs are predominantly produced via the Drell-Yan [1] process. In the Standard Model, quark-antiquark annihilations form an intermediate γ^* or Z (γ^*/Z) vector boson, which may yield an e^+e^- pair. The presence of both vector and axial-vector couplings in this process gives rise to a forward-backward asymmetry, A_{FB} , in the final-state angle of the *electron* in the rest frame of the e^+e^- pair (with respect to the *proton* direction). The Standard Model predicts accurately the mass $[M]$ dependence of the production cross section ($d\sigma/dM$) and A_{FB} . In the region of the Z resonance, the predicted asymmetry is related to the electroweak mixing angle. For $M \gg M_Z$, the large predicted asymmetry (near 0.6) is a consequence of the interference between the propagators of the γ^* and Z . Various new interactions not included in the Standard Model could result in deviations from the Standard Model predictions for both $d\sigma/dM$ and A_{FB} . Possible new interactions include additional gauge bosons [2–4], quark-lepton compositeness [5], exchange of R parity violating supersymmetric particles or leptoquarks, and extra-dimensions [6].

In this communication we extract measurements of $d\sigma/dM$ and improve the existing measurements of A_{FB} . The previous CDF measurements in the e^+e^- [5] and $\mu^+\mu^-$ [7] channels reported on a central ($|\eta| < 1.1$) region measurements of $d^2\sigma/dMdy$ averaged over rapidities [8] of $|y| < 1$. Electrons in the plug ($1.1 < |\eta| < 2.4$), but not forward ($2.2 < |\eta| < 4.2$) calorimeter were included in the previous CDF measurement [9] of A_{FB} , but backgrounds in the plug region were large resulting in significant uncertainties. This analysis includes electrons in the plug and forward regions of the calorimeter, thus covering a larger range of rapidity. New analysis techniques and tracking requirements in the forward region greatly reduce the backgrounds and uncertainties. In addition, by applying electroweak and QED radiative corrections [10,11] (which correct for the change in M from the emission of final state photons), measurements of A_{FB} in small bins over a large range in mass are extracted for the first time. Our measurement of e^+e^- pairs with invariant masses between 40 and 500 GeV/c^2 complement measurements of cross-sections and asymmetries in e^+e^- machines, which currently extend to 200 GeV/c^2 .

The e^+e^- pairs come from 108 pb^{-1} of $p\bar{p}$ collisions at $\sqrt{s} = 1.8 \text{ TeV}$ taken by the Collider Detector at Fermilab [8] (CDF) during 1992–1993 ($18.7 \pm 0.7 \text{ pb}^{-1}$) and

1994–1995 ($89.1 \pm 3.7 \text{ pb}^{-1}$). The CDF detector consists of a solenoidal magnetic spectrometer surrounded by projective-tower-geometry calorimeters and outer muon detectors. Only detector components used in this measurement are described here. Charged particle momenta and directions are measured by the spectrometer embedded in a 1.4 T axial magnetic field, an 84-layer cylindrical drift chamber (CTC), an inner vertex tracking chamber (VTX), and a silicon vertex detector (SVX). The polar coverage of the CTC tracking is $|\eta| < 1.2$. The $p\bar{p}$ collision point along the beam line (Z_{vertex}) is determined using tracks in the VTX. The energies and directions [8] of electrons, photons, and jets are measured by three separate calorimeters covering three regions: central, end plug, and forward. Each calorimeter has an electromagnetic (EM) and a hadronic (HAD) calorimeter. We follow the analysis procedure used in our previous measurements [12,13] of $d\sigma/dy$ and $d\sigma/dP_T$ of Z boson pairs. The measurement of A_{FB} requires the sign of at least one lepton. Therefore, we require one of the leptons to be in the central region.

The sample of e^+e^- events was collected by a three-level online trigger that required an electron in either the central or the plug calorimeter. The offline analysis selected events with two or more electron candidates. Since the electrons from the Drell-Yan process are typically isolated, a cut on the amount of transverse energy in a cone outside the electron shower is imposed. Electrons in the central, end plug, and forward regions are required to be within the fiducial area of the calorimeters and to have a minimum E_T of 22, 20, and 15 GeV, respectively. To improve the purity of the sample, electron identification cuts are applied [14]. The central electron (or one of them if there are two) is required to pass strict criteria. The criteria on the other electron are looser. A central electron must have a CTC track that extrapolates to the electron's shower cluster in the EM calorimeter. This cluster must have EM-like transverse shower profiles. The track momentum and the EM shower energy must be consistent with one another. The track is also used to determine the position and direction of the central electron. The fraction of energy in the HAD calorimeter towers behind the EM shower is required to be consistent with that expected for an EM shower ($E_{\text{HAD}}/E_{\text{EM}}$). The plug electrons must also have an EM-like transverse shower profile. The end plug and forward electrons are required to pass the $E_{\text{HAD}}/E_{\text{EM}}$ requirement and to have a track in the VTX which originates from the same vertex as the

other electron and points to the position of the electromagnetic cluster in the calorimeter. The ratio of found to expected hits in the VTX is required to be greater than 70% and 50% for plug and forward electrons, respectively. The VTX tracking efficiency is $(97.8 \pm 0.3)\%$ for plug electrons and $(97.0 \pm 0.9)\%$ for forward electrons. To further reduce the backgrounds from dijet events for very forward electrons both leptons legs for CF events are required to be on the same side of the detector i.e. have the same sign in η . The total data sample after all cuts consists of 7632 events.

With the above cuts, backgrounds are low and can be reliably estimated using the data. Because of the CTC tracking requirement, the jet background for the CC sample is negligible. All CC events are required to be opposite sign (the 8 same sign events are all in the Z mass region and originate from the small charge misidentification probability). The CC background is mainly composed of e^+e^- pairs from W^+W^- , $\tau^+\tau^-$, $c\bar{c}$, $b\bar{b}$, and $t\bar{t}$ sources. This background is estimated using $e^\pm\mu^\mp$ pairs. Because of the tracking and same side requirements, the backgrounds in the CP and CF topologies are also small and mainly come from dijets events. These are extracted from the data by fitting the isolation energy distribution to a sum of the expected distributions for signal and background events. For $M_{ee} > 105$ GeV the isolation energy fraction is used. The shapes of the isolation energy distributions are extracted from specially selected jet background-dominated and electron signal-dominated data samples.

The acceptance for Drell-Yan e^+e^- pairs is obtained using the Monte Carlo event generator PYTHIA 6.146 [15], and CDF detector simulation programs. PYTHIA generates the LO QCD interaction ($q + \bar{q} \rightarrow \gamma^*/Z$), simulates initial state QCD radiation via its parton shower algorithms, and generates the decay, $\gamma^*/Z \rightarrow e^+e^-$. To approximate higher order QCD corrections to the LO mass distribution, a K -factor [16] is used as an event weight: $K(M^2) = 1 + \frac{4}{3}(1 + \frac{4}{3}\pi^2)\alpha_s(M^2)/2\pi$, where α_s is the QCD coupling. This factor improves the agreement between the NLO and LO mass spectra. (For $M > 50$ GeV/ c^2 , $1.25 < K < 1.36$.) The CTEQ5L [17] PDFs are used in the acceptance calculations. Final state QED radiation [10] from the $\gamma^*/Z \rightarrow e^+e^-$ vertex is added by the PHOTOS [11] Monte Carlo program. The parameters of PYTHIA 6.146 are tuned [15] to fit experimentally measured transverse momentum [13] and rapidity distributions [12] of e^+e^- pairs in the Z region. Generated events are processed by CDF detector simulation programs and are reconstructed as data. The calorimetry energy scales, resolutions, cut efficiencies and corresponding errors used in the detector simulation are extracted from the data. Reconstructed Monte Carlo events are accepted if they pass the fiducial, kinematic, and mass cuts.

The angle of the electron is determined in the Collins-Soper [18] frame, which reduces the uncertainty in the angle introduced by the transverse momentum of the incom-

ing partons. We determine the cross sections $d\sigma^+/dM$ and $d\sigma^-/dM$ for forward and backward events, respectively. $d\sigma/dM$ (shown in Figure 1(a)) and A_{FB} (shown in Figure 1(b)) are extracted from the sum and difference of the forward and backward cross sections. The very small misidentification probability is handled as a dilution factor in A_{FB} . The CC, CP, and CF samples are combined and are binned in M , and $d\sigma/dM$ is given by

$$\frac{d\sigma}{dM} = \frac{N - B}{C_{rc}\Delta M \sum_r \mathcal{L}_r \epsilon A_r}.$$

Here, N is the number of observed events, B is the estimated background in a bin, C_{rc} is the radiative correction [10,11] factor to convert the measured cross sections to a Born level (one boson exchange) cross section, ΔM is the bin width, the sum r is over the 1992–1993 and 1994–1995 runs, \mathcal{L}_r is the integrated luminosity, and ϵA_r is the run's combined event selection efficiency and acceptance. The backgrounds subtracted from the event count are predicted using the data and background samples. Acceptances are calculated separately for CC, CP, and CF pairs. They are combined with the corresponding event selection efficiencies to give ϵA_r . A_r includes corrections for detector resolution smearing. Since the PYTHIA/PHOTOS [11] Monte Carlo includes radiative final state photons, the effects of the final state radiated photons are calculated together with the acceptance calculation. Also shown in Figure 1(a) are CDF dimuon results for $d\sigma/dM$ (which have not been previously published). These were extracted from the published dimuon [7] data ($d^2\sigma/dMdy$ for $|y| < 1$) by applying a correction using a QCD-NLO calculation [19] that describes our measured Z e^+e^- pair y distributions [12] over the entire kinematic range. The e^+e^- cross sections and asymmetries for $M_{ee} < 105$ GeV/ c^2 are given in Table I, and the higher mass data samples and backgrounds are summarized in Table II. We define \bar{M} to be the mass value for which the cross section is equal to the average cross section over each bin, as calculated from a NNLO theoretical prediction [20] for $d\sigma/dM$.

The systematic errors are determined from the following: statistical errors in the fits to the fractional background, variations in the background estimates using different methods, the background in the efficiency sample, the uncertainty in energy resolution of the calorimeter, the choice of PDFs, and the distribution of e^+e^- P_T used in the Monte Carlo event generator. Above the region of the Z mass, the total systematic errors are much smaller than the statistical errors, and the total errors shown in Table II are dominated by statistics. In the Z mass region, the systematic errors are less than half of the statistical error (as shown below). The $p\bar{p}$ collision luminosity is derived with CDF's beam-beam cross section, $\sigma_{BBC} = 51.15 \pm 1.60$ mb [21,22]. The luminosity error of 3.9% contains the σ_{BBC} error and uncertainties specific to running conditions. As described in a previous communication [12], the extracted cross section in the Z mass

region is $252.1 \pm 3.9(\text{stat.}) \pm 1.6(\text{syst.}) \pm 9.8(\text{lum.})$ pb. Note that since the $p\bar{p}$ inelastic cross section used by CDF in luminosity calculations differs from $D\bar{Q}$'s by +5.9% [22], the $D\bar{Q} e^+e^-$ cross sections [23] shown in Figure 1 have been multiplied by 1.059.

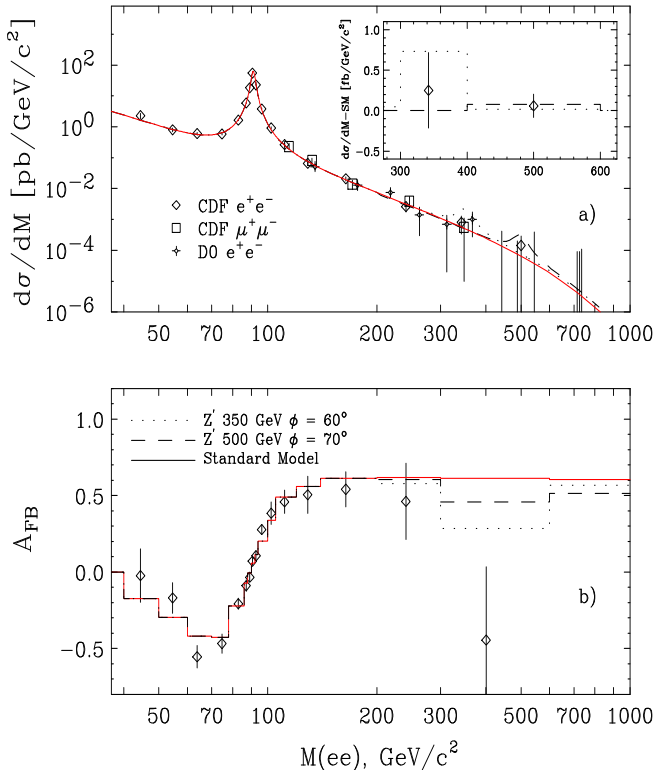


FIG. 1. (a) $d\sigma/dM$ distribution of e^+e^- and $\mu^+\mu^-$ pairs. All errors (except for the overall 3.9% luminosity error) have been combined in quadrature. The Standard Model theoretical predictions (solid line) have been normalized by a factor of 1.11 to the data in the Z boson mass region. Also shown are e^+e^- measurements from $D\bar{Q}$. (b) A_{FB} versus mass compared to the Standard Model expectation (solid line). Also, predicted theoretical curves for $d\sigma/dM$ and A_{FB} with an extra E_6 Z' boson (width of 10%) with $M_{Z'}=350$ (dotted line) and 500 GeV/c^2 (dashed line). The inset in (a) shows the difference between the $d\sigma/dM$ CDF data for e^+e^- pairs and the Standard Model prediction (on a linear scale) compared to expectation from these two Z' models.

Figure 1 also compares the measured $d\sigma/dM$ and A_{FB} to theoretical predictions. The $d\sigma/dM$ curve is a QCD NNLO [20] calculation with MRST99 NLO PDFs [24]. The predictions in Figure 1(a) are normalized by a factor $F=1.11$, the ratio of measured total cross section in the Z region to the NNLO prediction (the overall normalization uncertainties are 3.9% for the experimental data and 5% for the NNLO theory). The Standard Model predictions for A_{FB} have been calculated [3,10] in NLO-QCD. The measured $d\sigma/dM$ and A_{FB} values are in good agreement with the Standard Model predictions. However, A_{FB} in the highest mass bin (300-600 GeV/c^2) is 2.2σ (stan-

dard deviations) below the Standard Model prediction. There are three events [25] in the negative hemisphere and one event in the positive hemisphere. A negative asymmetry in this region could result from new interactions including additional gauge bosons [2–4] (discussed as an example below), quark-lepton compositeness [5], exchange of R parity violating supersymmetric particles, leptoquarks, and extra-dimensions [6]. For example, the predicted theoretical curves [3] for $d\sigma/dM$ and A_{FB} in models which include extra E_6 Z' bosons (with parameters tuned to fit low energy electroweak data) are shown as the dashed and dotted curves in Figure 1.

In summary, the measured $d\sigma/dM$ and A_{FB} values are in good agreement with the Standard Model predictions. At the highest mass values, the measured value of A_{FB} is 2σ lower than the Standard Model prediction. These high mass Drell-Yan data will be included in global fits to electroweak data to search (or extract limits) for physics beyond the Standard Model.

We thank the Fermilab staff and the technical staffs of the participating institutions for their vital contributions. This work was supported by the U.S. Department of Energy and National Science Foundation; the Italian Istituto Nazionale di Fisica Nucleare; the Ministry of Education, Science, Sports and Culture of Japan; the Natural Sciences and Engineering Research Council of Canada; the National Science Council of the Republic of China; the Swiss National Science Foundation; the A. P. Sloan Foundation; the Bundesministerium fuer Bildung und Forschung, Germany; the Korea Science and Engineering Foundation (KoSEF); the Korea Research Foundation; and the Comision Interministerial de Ciencia y Tecnologia, Spain.

-
- [1] S.D. Drell and T.-M. Yan, Phys. Rev. Lett. **25**, 316 (1970).
 - [2] J. Rosner, Phys. Rev. D **54**, 1078 (1996).
 - [3] A. Bodek and U. Baur, hep-ph/0102160 (January 2001).
 - [4] F. Abe *et al.*, Phys. Rev. Lett. **79**, 2192 (1997). M. Pillai, Ph.D. Thesis, Univ. of Rochester, UR1478 (1996).
 - [5] F. Abe *et al.*, Phys. Rev. Lett. **79**, 2198 (1997).
 - [6] H. Davoudiasl, J. L. Hewett, and T. G. Rizzo, Phys. Rev. Lett. **84**, 2080 (2000).
 - [7] F. Abe *et al.*, Phys. Rev. D **59**, 052002 (1999).
 - [8] F. Abe *et al.*, Nucl. Instrum. Methods Phys. Res. Sect. A **271**, 387 (1988). CDF coordinates are in (θ, ϕ, z) , where θ is the polar angle relative to the proton beam (the $+z$ axis), and ϕ the azimuth. The pseudorapidity is $\eta = -\ln \tan(\theta/2)$. Here $P_T = P \sin \theta$, $y = \frac{1}{2} \ln \frac{P_+ P_-}{P_- P_+}$, P and P_z are the magnitude and z component of a particle's momentum, and $E_T = E \sin \theta$, where E is the energy measured in the calorimeter.
 - [9] F. Abe *et al.*, Phys. Rev. Lett. **77**, 2616 (1996).

- [10] U. Baur, S. Keller, and W. K. Sakumoto, Phys. Rev. D **57**, 199 (1998).
- [11] E. Barberio and Z. Was, Comput. Phys. Commun. **79**, 291 (1994); E. Barberio, B. van Eijk, and Z. Was, *ibid.* **66**, 115 (1991).
- [12] T. Affolder *et al.*, Phys. Rev. D **63**, 011101(R) (2001); J. B. Liu, Ph.D. Thesis, Univ. of Rochester, UR1606 (2000).
- [13] T. Affolder *et al.*, Phys. Rev. Lett. **84**, 845 (2000).
- [14] The CDF top-quark high- P_T dilepton selection (F. Abe *et al.*, Phys. Rev. D **50**, 2966 (1994)) is used, but with both leptons isolated and no jet cuts.
- [15] T. Sjöstrand, Comput. Phys. Commun. **82**, 74 (1994). The default PYTHIA 6.146 is used except MSTJ(41)=1, MSTP(91)=1 and PARP(62,91,92)=2.25,2.0,10.0 GeV.
- [16] G. Altarelli, R. E. Ellis, and G. Martinelli, Nucl. Phys. B **157**, 461 (1979).
- [17] H. L. Lai *et al.*, Eur. Phys. J. C **12**, 375 (2000).
- [18] J. Collins and D. Soper, Phys. Rev. D **16**, 2219 (1977).
- [19] P. J. Rijken and W. L. van Neerven, Phys. Rev. D **51**, 44 (1995).
- [20] $\overline{\text{MS}}$: R. Hamberg, W.L. van Neerven, and T. Matsuura, Nucl. Phys. B **359**, 343 (1991). DIS :W. L. Van Neerven and E. B. Zijlstra, Nucl. Phys. B **382**, 11 (1992).
- [21] F. Abe *et al.*, Phys. Rev. Lett. **76**, 3070 (1996).
- [22] D. Cronin-Hennessy *et al.*, Nucl. Instrum. Methods Phys. Res., Sect. A **443/1**, 37-50 (2000).
- [23] B. Abbott *et al.*, Phys. Rev. Lett. **82**, 4769 (2000).
- [24] A.D. Martin *et al.*, Eur. Phys. J. C **14** 133 (2000).
- [25] The (mass, $\cos\theta$, region) of the four highest mass ee events are (303,0.4,CP), (319,-0.41,CC), (354,-0.14,CC), and (496,-0.29,CC), respectively. Because of acceptance of the muon chambers is limited to the central region, a good measurement of A_{FB} cannot be done in this channel. Nonetheless, the three highest mass dimuon events (292, 300, and 320 GeV) all have positive $\cos\theta$.

TABLE I. The e^+e^- cross sections and asymmetries for $M_{ee} < 105 \text{ GeV}/c^2$. The statistical and systematic errors have been combined in quadrature. The 3.9% overall luminosity error is not included.

Mass Bin (GeV/ c^2)	\overline{M}_{ee} (GeV/ c^2)	$d\sigma_{ee}/dM$ (pb/GeV/ c^2)	A_{FB}
40 – 50	44.5	2.30 ± 0.47	-0.02 ± 0.17
50 – 60	54.6	0.80 ± 0.11	-0.17 ± 0.10
60 – 70	63.8	0.60 ± 0.06	-0.56 ± 0.07
70 – 78	74.7	0.58 ± 0.05	-0.47 ± 0.06
78 – 86	82.9	1.64 ± 0.06	-0.21 ± 0.04
86 – 88	87.1	5.89 ± 0.22	-0.09 ± 0.04
88 – 90	89.2	18.28 ± 0.52	-0.04 ± 0.03
90 – 92	90.6	54.85 ± 1.39	0.07 ± 0.02
92 – 94	92.8	22.75 ± 0.66	0.11 ± 0.03
94 – 100	96.2	3.80 ± 0.12	0.28 ± 0.03
100 – 105	102.2	0.91 ± 0.07	0.38 ± 0.07

TABLE II. The number of signal and background events and correction factors involving the extraction of $d\sigma_{ee}^+/dM$, $d\sigma_{ee}^-/dM$, $d\sigma_{ee}/dM$, and $d\sigma_{\mu\mu}/dM$ for mass bins above the Z pole. Here, N is the number of events, B is the background estimate, ϵAC_{rc} is the combined efficiency, acceptance, smearing and radiative correction. The statistical and systematic errors for $d\sigma/dM$ have been combined in quadrature. The 3.9% overall luminosity error is not included.

Mass Bin (GeV/ c^2)	\overline{M}_{ee} (GeV/ c^2)	N	B	ϵAC_{rc}	$d\sigma_{ee}^+/dM$ (fb/GeV/ c^2)
105 – 120	111.2	93	2.3	0.293	191.55 ± 20.38
120 – 140	128.8	34	1.4	0.307	49.20 ± 8.81
140 – 200	164.2	35	1.2	0.326	16.01 ± 2.80
200 – 300	240.6	7	0.1	0.337	1.88 ± 0.73
300 – 400	343.2	1	0.0	0.330	0.28 ± 0.28
400 – 600	478.8	0	0.0	0.307	0.00 ± 0.15
600 – 999	725.6	0	0.0	0.227	0.00 ± 0.10
Mass Bin	\overline{M}_{ee}	N	B	ϵAC_{rc}	$d\sigma_{ee}^-/dM$
105 – 120	111.2	39	2.3	0.321	70.64 ± 12.04
120 – 140	128.8	13	1.4	0.334	16.07 ± 5.01
140 – 200	164.2	12	1.2	0.353	4.74 ± 1.52
200 – 300	240.6	3	0.1	0.386	0.69 ± 0.42
300 – 400	343.2	2	0.0	0.398	0.47 ± 0.33
400 – 600	478.8	1	0.0	0.391	0.12 ± 0.12
600 – 999	725.6	0	0.0	0.355	0.00 ± 0.07
Mass Bin	\overline{M}_{ee}	N	B	ϵAC_{rc}	$d\sigma_{ee}/dM$
105 – 120	111.2	132	4.7	0.300	262.29 ± 23.67
120 – 140	128.8	47	2.9	0.313	65.46 ± 10.17
140 – 200	164.2	47	2.4	0.331	20.81 ± 3.20
200 – 300	240.6	10	0.3	0.346	2.60 ± 0.85
300 – 400	342.2	3	0.0	0.343	0.81 ± 0.47
400 – 600	478.8	1	0.0	0.324	0.14 ± 0.14
600 – 999	725.6	0	0.0	0.252	0.00 ± 0.09
Mass Bin	$\overline{M}_{\mu\mu}$	N	B	ϵAC_{rc}	$d\sigma_{\mu\mu}/dM$
110 – 120	114.5	29	0	0.181	231.93 ± 51.56
120 – 150	132.5	28	0	0.167	80.61 ± 15.93
150 – 200	171.2	9	0	0.164	13.98 ± 4.67
200 – 300	240.6	6	0	0.168	3.91 ± 1.58
300 – 400	343.2	1	0	0.176	0.56 ± 0.56
400 – 600	478.8	0	0	0.227	0.00 ± 0.20
600 – 999	725.6	0	0	0.230	0.00 ± 0.11